Available online at www.sciencedirect.com
SCIENCE DIRECT®
Acta Materialia 52 (2004) 1899–1907
Acta MATERIALIA
www.actamat-journals.com

Texture changes in the hcp → bcc → hcp transformation of zirconium studied in situ by neutron diffraction

H.-R. Wenk [a,*], I. Lonardelli [a], D. Williams [b]

[a] Department of Earth and Planetary Science, University of California, McCone Hall, Berkeley, CA 94720, USA
[b] Lujan Center, Los Alamos National Laboratory, Los Alamos, NM 87545, USA

Received 15 September 2003; received in revised form 15 December 2003; accepted 16 December 2003

Abstract

The crystallographic texture of hot-rolled polycrystalline zirconium has been studied below and above the hcp–bcc transition temperature with HIPPO, the new time-of-flight neutron diffractometer at Los Alamos Neutron Science Center, making use of the multidetector capabilities and a vacuum furnace. Incomplete pole figures were extracted from diffraction spectra to determine the orientation distribution function and recalculate complete pole figures in situ at various temperatures. The texture analysis reveals that the orientation of grains in the new high-temperature (bcc) phase is related to the texture of the low-temperature (hcp) phase by Burgers relation, but with both an orientation selection and a symmetry variant selection. The cubic transformation texture is best explained if we assume preferential nucleation of the bcc phase in the hcp grain orientations that are most subject to mechanical twinning. After cooling, the new hcp texture closely resembles the original texture. Thermal cycling repeats this process with slight strengthening of the texture. The hexagonal transformation texture (after cooling) may be caused by nucleation and growth of untransformed domains or through variant selection by stresses imposed by neighboring grains.

Keywords: Zirconium; Texture; Phase transformation (hcp–bcc); Variant selection; Neutron diffraction

1. Introduction

When heated to temperatures higher than about 860 °C, the hexagonal metals zirconium and titanium, both undergo a transformation from a hcp (α) to a bcc (β) structure. Burgers [1] proposed an orientation relationship based on structural similarities. According to him a fairly dense-packed $\{0\,1\,1\}$ plane of the bcc lattice is parallel to the closest-packed $(0\,0\,0\,1)$ plane of the hcp lattice and a nearest neighbor $\langle 1\,\bar{1}\,1\rangle$ direction in the bcc lattice is parallel to a nearest neighbor $\langle 1\,1\,\bar{2}\,0\rangle$ direction in the hcp lattice. The orientation, which corresponds to a coincidence lattice relationship [2], was confirmed for single crystals [1,3–5]. For single crystals, lattice vibration studies revealed a martensitic mechanism for the transformation under some conditions [6–8] and an equivalent lattice relationship that better corresponds to the martensitic mechanism was proposed [9] ($\{1\,\bar{1}\,0\,0\}\langle 1\,1\,\bar{2}\,0\rangle$(hcp) → $\{1\,\bar{1}\,2\}\langle\bar{1}\,1\,1\rangle$(bcc)). As the crystal transforms from hcp to bcc, there are six symmetrically equivalent orientation variants and as the bcc crystal returns to hcp after cooling, there are 12 equivalent hcp variants. Jourdan et al. [5] showed a distinct memory effect, i.e., the crystal returned to the same orientation from which it started.

Orientation changes during the phase transformation were also investigated in deformed polycrystalline aggregates. Several researchers have observed that when zirconium and titanium with a strong rolling texture are heated above the transition temperature and then cooled again, the resulting hcp texture is similar to the starting texture [10–14], also in this case suggesting a variant selection, that was shown to depend on the initial microstructure. Since the bcc phase cannot be quenched to room temperature, the bcc transformation texture can only be studied at temperatures higher than about

* Corresponding author. Tel.: +1-510-642-7431; fax: +1-510-643-9980.
E-mail address: wenk@seismo.berkeley.edu (H.-R. Wenk).

1359-6454/$30.00 © 2004 Acta Materialia Inc. Published by Elsevier Ltd. All rights reserved.
doi:10.1016/j.actamat.2003.12.029

860 °C, and such measurements are very difficult. Indeed, most of the existing work is limited to calculating the bcc texture pattern from the hcp textures, either before heating or after the bcc–hcp re-transformation, using the Burgers orientation relation [10,13,15] and making some assumptions. The few reports on experimentally determined orientation distributions of the bcc phase are ambiguous [14,16]. In polycrystals it has been established that the transformation occurs largely by nucleation and growth, rather than simple shear displacements, particularly through direct in situ observations with an SEM [16].

The present high-temperature neutron diffraction study was undertaken to take advantage of new experimental capabilities and measure the bcc texture directly at high temperature and determine the variant selection in both hcp → bcc and bcc → hcp transformations experimentally in polycrystalline zirconium. In this report we will first describe the experiment and data processing, then present the results and finally apply modelling to quantify the variant selection and propose a plausible explanation.

2. Experiment and data processing

The sample used in the present study was a $6 \times 6 \times 6$ mm^3 cube of hot rolled Zircaloy-4 (thickness reduction = 80%). Material of this type is commonly used in the fuel cladding of pressurized water nuclear reactors, and alloyed elements typically include 1.3 wt% Sn, 0.2 wt% Fe and 0.1% Cr. Microscopic inspection of the specimen showed lamellar grains of a length on the order of 50 μm and a height of about 10 μm aligned with the long axis in the rolling direction (RD) and indicated the presence of some equiaxed recrystallized domains inside the lamellae.

The texture measurements were performed on the new time-of-flight (TOF) HIPPO (high pressure preferred orientation) diffractometer at the Los Alamos Neutron Science Center (LANSCE). The HIPPO diffractometer is equipped with a large number of detector panels positioned at different angles and each detector views a set of differently oriented crystals. Detectors are arranged on rings at different diffraction angles θ. For the present study, only the 150° bank (eight detectors), the 90° bank (10 detectors) and the 40° bank (12 detectors) were used. With the TOF technique, the data acquisition time is reduced since spectra with many hkl diffraction peaks are measured simultaneously [17]. For the present study, the sample was mounted in a vacuum furnace with Nb heating elements that was available at LANSCE. It is designed to minimize thermal gradients using a high aspect ratio tube geometry and multiple Nb heat reflectors surrounding the sample. Minimal thermal gradients on the scale of the analyzed sample volume are essential in phase transformation studies to achieve a macroscopically homogeneous transformation. A disadvantage of the Nb heating elements and heat reflectors is that they produce strong diffraction peaks that partly overlap with the signal obtained from the sample and preclude the use of certain hkl reflections and some of the 30 available detectors for the texture analysis.

Two subsequent heating–cooling cycles were carried out, and diffraction spectra were measured at different temperatures in the sequence 25 °C (hcp)–750 °C (hcp)–850 °C (hcp)–950 °C (bcc)–750 °C (hcp)–950 °C (bcc)–750 °C (hcp) over a time period of about 7 h (Table 1). Heating rates were on the order of 20 K/min; cooling, particularly to lower temperatures, was much slower. Fig. 1 shows diffraction spectra obtained from a 150° detector at two different temperatures, 750 and 950 °C. Diffraction peaks used for the texture analysis are indexed and illustrate that the phase transformation has indeed occurred. An arrow denotes a small residual $(10\bar{1}1)$ hcp-Zr peak in the high temperature spectrum, indicating that the sample has not completely trans-

Table 1
Experimental details and texture information

#	Temperature (°C)	Time (end of data collection)	ODF Max (m.r.d.)	Texture index
X-ray	25		3.59	1.53
1	40	21:00		
2	750	22:16	5.31	2.05
3	850	23:35		
4	950	00:53	5.20	1.73
5	750	02:10	4.17	1.59
6	950	03:38	7.71	1.81
7	750	04:54	5.87	1.82
8	200	06:35		

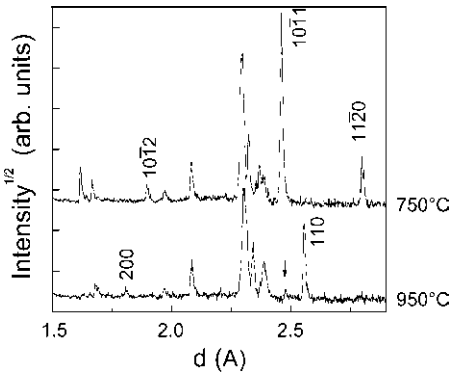

Fig. 1. Neutron diffraction patterns obtained from rolled zirconium at 750 °C (hcp phase) and 950 °C (bcc phase). Diffraction peaks without hkl indices are dominated by beam interaction with the high-temperature Nb furnace. Indexed diffraction peaks have been used for the texture analysis. The arrow indicates a small residual fraction of hcp Zr in the bcc-transformed sample.

formed into bcc after heating at 950 °C. (In order to avoid any ambiguities about phase identification we are using three-index Miller indices for bcc and four-index Miller–Bravais indices for hcp). Also visible on the diffraction pattern are diffraction peaks from the furnace.

To improve the pole figure coverage, diffraction spectra were measured in six different sample orientations by rotating the sample around the furnace axis (perpendicular to the neutron beam) in 60° increments. Each measurement took 8 min, resulting in a measuring time for a temperature step of about 1 h. Table 1 gives a log of the experiments with temperature and time. The time is significant because microstructural changes may occur at one thermal step.

The diffraction spectra obtained from the different detectors were corrected for the energy spectrum of the incident neutron beam and integrated intensities of different $h\,k\,l$ peaks were extracted from the spectra with an automated peak fitting software. Due to strong overlaps of some diffraction peaks with parasitic peaks arising from the furnace material, the coverage is limited and many peak intensities had to be rejected. The extracted intensities were normalized by the signal obtained from a (random texture) Si powder measured in the furnace prior to the Zr sample to account for counting efficiency variations between different detectors, as well as for intensity variations caused by different absorption path lengths of the diffracted neutrons in the furnace material as a function of the detector position. Pole figure coordinates were calculated from the detector positions and sample rotation angles, respectively, and assigned to the extracted peak intensities to yield experimental pole densities. The pole densities were then used to calculate the grain orientation distribution function (ODF) of the sample for each temperature using a modified WIMV (Williams–Imhof–Matthies–Vinel) algorithm [18] capable of processing incomplete pole density distributions on irregular coordinate grids as the one provided by the HIPPO instrument and implemented in the software package MAUD (materials analysis using diffraction) [17,19]. A $10° \times 10° \times 10°$ grid was used for the computation of the ODF, and the tube projection technique [20] was used to account for the low experimental pole figure coverage – in particular that of the bcc phase. No sample symmetry was imposed. Complete pole figures for both structural phases and all $h\,k\,l$ of interest were recalculated from the ODF to facilitate the discussion of the observed orientation changes. Such pole figures are internally consistent with the ODF. In the following, these pole figures, recalculated from the experimental data, will be referred to as 'experimental' pole figures to distinguish them from simulated texture patterns. For various transformations, representations and modelling, use was made of the software package BEARTEX [21].

3. Results

Pole figures for the starting material, measured ex situ with an X-ray pole figure goniometer, are shown in Fig. 2(a). Experimental pole figures extracted from the neutron diffraction data for hexagonal zirconium 750 °C at different thermal cycles are shown in Figs. 2(b) and (d). In the figures the transverse direction (TD) is pointing up and the RD is pointing to the right. The same logarithmic grey scale used for the display of all measurements is in units of multiples of the random distribution (m.r.d.). Some details about the texture such as texture index and maximal orientation densities are also summarized in Table 1.

All pole figures display more or less orthorhombic symmetry, consistent with the deformation conditions. We attribute deviations from this symmetry to limitations of the experiment, particularly the highly incomplete pole figure coverage. The dominant feature of the initial hexagonal texture is a broad (0 0 0 1) maximum in the normal direction (Fig. 2(a)). This maximum is spread out towards the transverse direction. The $(1\,0\,\bar{1}\,0)$ pole figure shows in the starting material a maximum in the rolling direction. The neutron texture at 750 °C (Fig. 2(b)) is similar to the X-ray texture (Fig. 2(a)), which gives us confidence that neutron data processing procedures are correct. $(1\,1\,\bar{2}\,0)$ pole figures also have a maximum in the rolling direction, but it is initially broader than the $(1\,0\,\bar{1}\,0)$ maximum and extended towards the transverse direction (Fig. 2(b)).

After the first heating cycle into the cubic phase (above 950 °C) and cooling back to 750 °C, the material is largely hexagonal again, with a similar texture pattern as in the starting material. The texture is slightly stronger and the (0 0 0 1) maximum splits more distinctly into two submaxima (Fig. 2(c)). The main difference is that the new hcp texture has a distinct $(1\,1\,\bar{2}\,0)$ maximum in the rolling direction and the $(1\,0\,\bar{1}\,0)$ maximum is spread out. The subsequent second heating–cooling cycle (Fig. 2(d)) resulted in similar texture patterns as the first one. The split (0 0 0 1) maxima are still better defined and at higher angles to the rolling direction and the $(1\,1\,\bar{2}\,0)$ maximum in the rolling direction is very distinct. At the same time, the $(1\,0\,\bar{1}\,0)$ maximum in the rolling direction becomes more spread out. There is some texture strengthening as indicated by the texture index and the ODF maximum (Table 1).

Above 850 °C, the material transforms largely to bcc, with only very small amounts of hcp remaining (Fig. 1, bottom). To our knowledge the bcc textures of zirconium at 950 °C in Fig. 3 is the first reported experimental transformation textures of that material. The most distinct feature of the bcc texture is a (1 1 1) maximum in the rolling direction (Fig. 3(a)). The (1 0 0) and (1 1 0) pole figures look more complicated, with many submaxima arranged on small circle girdles

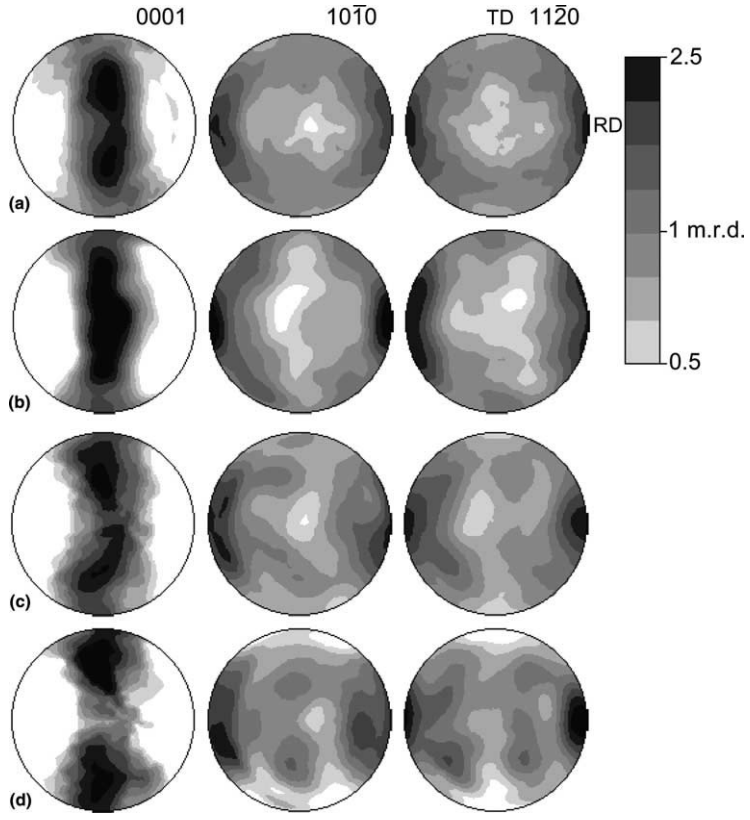

Fig. 2. Experimental pole figures of hexagonal Zr obtained during thermal cycling (cf. Table 1). (a) Room temperature, (b) 750 °C (before phase transformation), (c) 750 °C (after phase transformation), (d) 750 °C (after second phase transformation). Equal area projection, rolling direction (RD) and transverse direction (TD) are indicated. (a) Measured with an X-ray pole figure goniometer, (b)–(d) with TOF neutron diffraction.

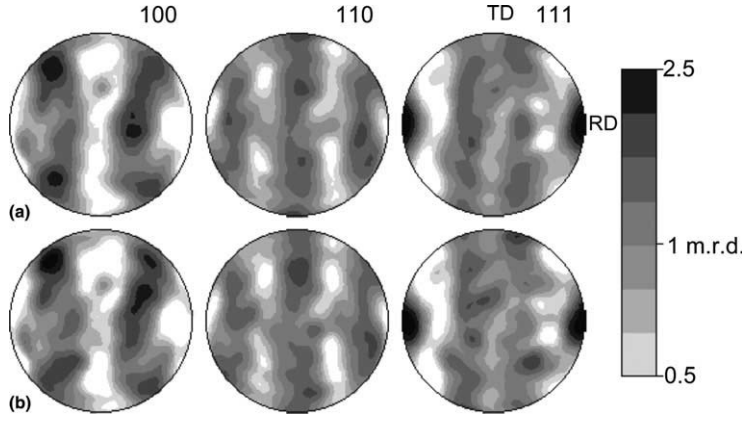

Fig. 3. Experimental pole figures of cubic Zr obtained measured in situ at 950 °C with TOF neutron diffraction. (a) First heating cycle, (b) second heating cycle. Equal area projection, rolling direction (RD) and transverse direction (TD) are indicated.

around the rolling direction. After a second heating cycle to 950 °C, the bcc texture is very similar as during the first cycle, though slightly stronger (Fig. 3(b)).

4. Discussion

This study presents the first reliable experimental data for the bcc transformation texture of zirconium. The observed bcc texture is different from that previously implied from modelling [10,12]. For example, the strong (1 0 0) maximum in the rolling direction in the modelled textures [13] is clearly absent in the experimental bcc texture pattern.

The texture of the starting material, measured by X-ray as well as neutron diffraction, is similar to that observed by other workers for rolled zircaloy [10] and titanium [22,23]. During annealing prior to the phase

transformation there are minor, but significant changes. A texture component with c axes about 30° from the normal direction and a axes $(1\,1\,\bar{2}\,0)$ in the rolling direction preferentially develops. Similar changes that occur during recrystallization have been documented for titanium and were represented in difference pole figures [24,25].

Previous workers have also observed a similar memory effect when the bcc texture returns to hcp, though without being able to measure the bcc texture. Differences in the back-transformed hcp texture from the initial hcp texture were correlated with microstructural differences [12]. From all this work on polycrystalline zirconium and titanium it is clear that nucleation and growth play an important role, not only during recrystallization, but during the phase transformation as well, consistent with electron microscope observations [16,24].

In order to investigate more closely the crystallographic relationships between parent and daughter textures, we did some modelling. As a first step we have first decomposed the hcp texture into ideal components. Initially, during low temperature rolling the principal component is $g_1 = \{\alpha = 90°,\ \beta = 0°,\ \gamma = 0°\}$ (where α, β and γ are Euler angles in Matthies–Roe convention [18]), an orientation with the c-axis pointing in the normal direction (ND) and $(1\,0\,\bar{1}\,0)$ poles in the RD. A $(1\,1\,\bar{2}\,0)$ pole figure is shown in Fig. 4(a). With further rolling and annealing the c-axis maximum is displaced towards the transverse direction, which can be described by component $g_2 = \{\alpha = 90°,\ \beta = 30°,\ \gamma = 0°\}$ (Fig. 4(b)). During annealing, there is also a rotation of the texture about the c-axis as described by a third component $g_3 = \{\alpha = 90°,\ \beta = 30°,\ \gamma = 30°\}$ with $(1\,1\,\bar{2}\,0)$ in the rolling direction. There is a fourth component with c axes at yet higher angles $g_4 = \{\alpha = 90°,\ \beta = 45°,\ \gamma = 0°\}$. We have not used it for calculating the composite texture because, as we will later see, component 3 is of most interest for the phase transformation.

With components 1–3 (treating them as spherical in Euler space), assigning volume fractions and Gauss widths of 45° (Table 2), we calculated an orientation distribution and from it recalculated pole figures that are displayed in Figs. 4(d)–(f). Orthorhombic sample symmetry was applied to all components. These pole figures resemble closely those that have been measured (Figs. 2(a) and (b)), not only in pattern but also in texture strength. Main features are a split $(0\,0\,0\,1)$ maximum in the normal direction and spread out $(1\,0\,\bar{1}\,0)$ and $(1\,1\,\bar{2}\,0)$ maxima in the rolling direction.

For the analysis of the transformation texture we relied on Burgers relationships with the bcc $\{0\,1\,1\}$ planes aligning parallel to the hexagonal close-packed $(0\,0\,0\,1)$ plane and a cubic nearest neighbor $\langle\bar{1}\,1\,\bar{1}\rangle$ direction parallel to a hexagonal nearest neighbor $\langle\bar{2}\,1\,1\,0\rangle$ direction. Six symmetrically equivalent variants of this orientation relationship exist and can in principle occur in the hcp → bcc texture transformation (Table 3). For the reverse transformation (bcc → hcp) there are 12 possible variants. Note that the symmetry equivalence only refers to crystal symmetry, not to sample symmetry and microstructural characteristics. Each of the six variants can be represented as a matrix operator transforming a hcp parent crystallite orientation $\{\alpha, \beta, \gamma\}$ into a bcc daughter orientation $\{\alpha', \beta', \gamma'\}$. For the transformation the definition of coordinate systems is essential

Table 2
Ideal crystal orientations used to describe the experimental hcp texture patterns

Texture component	Euler angles (°)			Volume fraction
	α	β	γ	
g_1	90	0	0	0.1 (Fig. 4(a))
g_2	90	30	0	0.6 (Fig. 4(b))
g_3	90	30	30	0.3 (Fig. 4(c))
g_4	90	45	0	–

The volume fractions have been used to simulate the pole figures in Figs. 4(d)–(f).

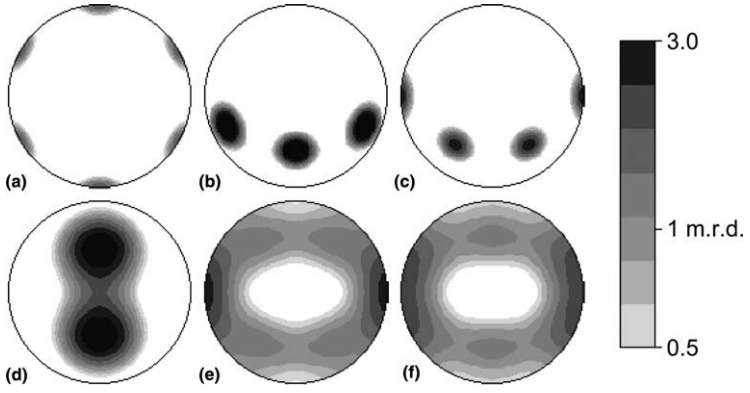

Fig. 4. Ideal components of the hcp texture. (a) $1\,1\,\bar{2}\,0$ pole figure for component g_1, (b) $1\,1\,\bar{2}\,0$ pole figure for g_2, (c) $1\,1\,\bar{2}\,0$ pole figure for g_3, (d) $0\,0\,0\,1$ pole figure with all three components added for volume fractions defined in Table 2, (e) $1\,0\,\bar{1}\,0$ pole figure, (f) $1\,1\,\bar{2}\,0$ pole figure. Equal area projection.

Table 3
Burgers orientation variants for the hcp–bcc texture transformation with corresponding Euler angles referred to the hexagonal crystal (Figs. 5 and 6)

Variant index	Burgers relations		Euler angles (bcc in hcp system)		
	Plane $(\alpha)\|\|(\beta)$	Direction $[\alpha]\|\|[\beta]$	α	β	γ
1	(0 0 0 1) (0 1 $\bar{1}$)	[$\bar{2}$ 1 1 0] [$\bar{1}$ 1 $\bar{1}$]	144.7	45	0
2	(0 0 0 1) (0 $\bar{1}$ $\bar{1}$)	[$\bar{2}$ 1 1 0] [$\bar{1}$ 1 $\bar{1}$]	−144.7	45	0
3	(0 0 0 1) (0 1 $\bar{1}$)	[1 1 $\bar{2}$ 0] [$\bar{1}$ 1 $\bar{1}$]	204.7	45	0
4	(0 0 0 1) (0 $\bar{1}$ $\bar{1}$)	[1 1 $\bar{2}$ 0] [$\bar{1}$ 1 $\bar{1}$]	−204.7	45	0
5	(0 0 0 1) (0 1 $\bar{1}$)	[1 $\bar{2}$ 1 0] [$\bar{1}$ 1 $\bar{1}$]	264.7	45	0
6	(0 0 0 1) (0 $\bar{1}$ $\bar{1}$)	[1 $\bar{2}$ 1 0] [$\bar{1}$ 1 $\bar{1}$]	−264.7	45	0

and, since there are several conventions, the one used in this study is shown in Fig. 5. This Figure illustrates the orientation of bcc variant 1 (Euler angles $\alpha' = 145°,\ \beta' = 45°,\ \gamma' = 0°$) relative to the hcp crystal in the standard orientation in coordinate system X, Y, Z. In Fig. 6, the transformation is applied to some of the components defined in Table 2. Fig. 6(a) applies a single variant (1) to component g_1. Fig. 6(b) applies all six variants to component g_1. Numbers for variants are assigned corresponding to Table 3. (Notice that $g_1 = \{\alpha = 90°,\ \beta = 0°,\ \gamma = 0°\}$ is equivalent to $\{\alpha = 0°,\ \beta = 0°,\ \gamma = 30°\}$). In this pattern we note a (1 1 0) maximum in the normal direction (for all six components) and a (1 1 1) maximum in the rolling direction (for components 1, 2, 3 and 6). Finally, Fig. 6(c) applies all variants to component g_3 (corresponding to a rotation around the rolling direction). In the latter pole figures we observe a strong (1 1 1) maximum in the rolling direction (again components 1, 2, 3 and 6), as in the experimental bcc pole figures (Fig. 3) and a maximum for (1 1 0) that is inclined to the rolling direction (for all components).

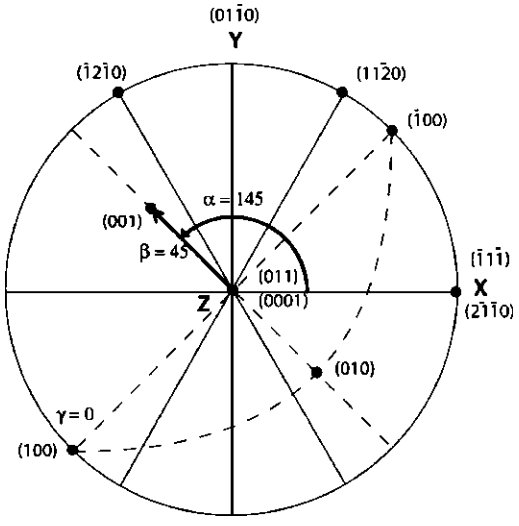

Fig. 5. Definition of coordinate system and of Euler angles α, β and γ for hcp and bcc crystals. The hcp crystal is in the standard orthogonal coordinate system X, Y, Z. For bcc the orientation variant 1 $\{\alpha' = 145°,\ \beta' = 45°,\ \gamma' = 0°\}$ is shown relative to the hcp crystal.

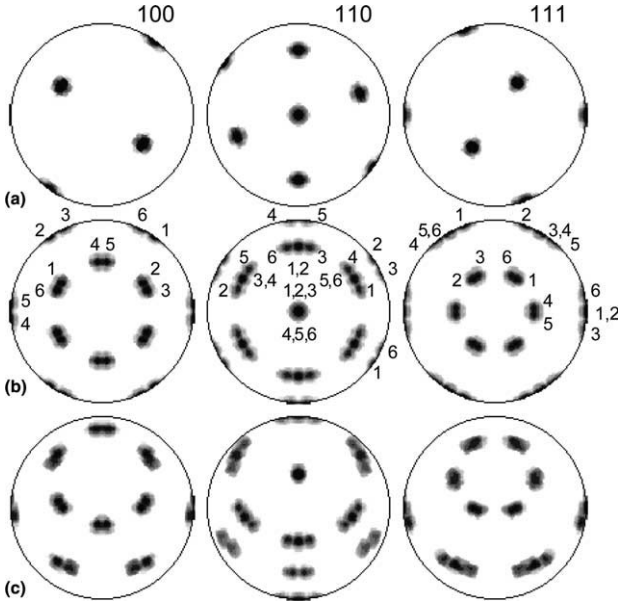

Fig. 6. The bcc components based on hcp texture components (Table 2, Fig. 4) applying Burgers relation and represented as (1 0 0), (1 1 0) and (1 1 1) pole figures. (a) Single symmetry variant (1 in Table 3, $\{\alpha' = 145°,\ \beta' = 45°,\ \gamma' = 0°\}$) for grain orientation $\{\alpha = 90°,\ \beta = 0°,\ \gamma = 30°\} = \{\alpha = 0°,\ \beta = 0°,\ \gamma = 0°\}$. (b) All six symmetry variants applied to this orientation. The numbers refer to variants in Table 3. (c) All six symmetry variants applied to orientation $g_3\{\alpha = 90°,\ \beta = 30°,\ \gamma = 30°\}$. Equal area projection.

A next step is to apply all variants to the actual hexagonal grain orientations. This was done by assigning texture weights, based on the hcp ODF, to a set of 5000 random orientations, and then applying to each the six transformations, resulting in 30,000 weighted orientations. These served to prepare a continuous orientation distribution from which bcc pole figures were recalculated (Fig. 7(a)). The generated texture is very weak (texture index 1.02) and very different from the observed texture, indicating that selection rules must exist during the hcp → bcc phase transformation. These selections could either be grain orientation selections (e.g., components, Table 2) or symmetry variant selections (among equivalent variants, Table 3).

We tried many possibilities and most did not result in much agreement with experiments. However, one case did produce good agreement. Let us return to Fig. 6(c), where the transformation is applied to component g_3. When applying orthorhombic sample symmetry, there is qualitative agreement for (1 1 1), with the maximum in the rolling direction that is the most distinct characteristic of the experimental transformation texture. Four symmetry variants contribute to this texture maximum (1, 2, 3 and 6). Thus, in Fig. 7(b) the transformation was only applied to orientations of the experimental hcp

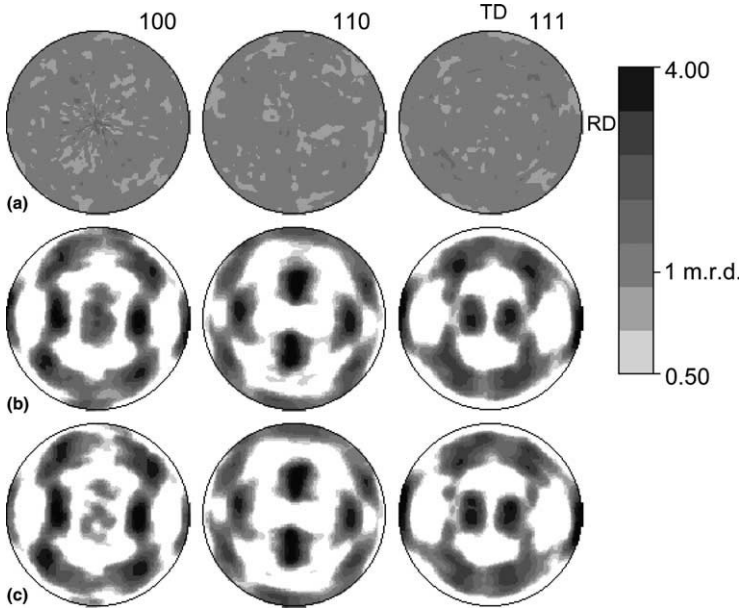

Fig. 7. Simulated bcc pole figures obtained from the hcp texture in Fig. 3(b), based on Burgers relation. (a) Transformation texture applied to all orientations with all six symmetry variants. (b) Transformation applied to orientations near g_3, without variant selection. (c) Transformation applied to orientations near g_3, with variant selection as described in the text. Equal area projection.

texture close to g_3 ($75° < \alpha < 105°$; $15° < \beta < 45°$; $15° < \gamma < 45°$). This grain orientation selection greatly improved the agreement. The (1 1 1) maximum in the rolling direction is present, as well as the oblique (1 1 0) maximum between transverse and normal direction that are both present in the experimental pole figures (Figs. 3(a) and (b)). However, this model also predicts a texture with a (1 0 0) maximum in the normal as well as in the rolling directions, which was also modelled by [10,12] but is not observed. As a second condition we have suppressed two of the six Burgers variants, those with (1 0 0) close to the normal direction (variants 4 and 5 in Fig. 6 that do not contribute to the (1 1 1) maximum in the rolling direction), and thereby obtain better agreement with experiments (Fig. 7(c) versus Figs. 3(a) and (b)).

From this geometric reasoning it appears that the observed bcc texture can be explained as a transformation from the hcp texture with Burgers relation applied but only if selection conditions are applied. A first condition refers to the original hcp grain orientation. Only certain orientations are selected. Perhaps those orientations have characteristics that are favourable for nucleation and with subsequent growth of the bcc phase they dominate the texture. A second condition is a symmetry variant selection and the data suggest that for the chosen orientations only four of the six equivalent variants are applied. At this point we have no quantitative explanation for these selections. Nevertheless there are some intriguing correspondences. Let us first speculate about the grain orientation selection. Is there any reason why component g_3 should dominate the transformation texture? Interestingly, this is also the preferred recrystallization component in titanium [24,25]. TEM investigations distinguished two microstructures in rolled titanium, one with large grains corresponding to orientation g_4 and one with heterogeneous divided grains corresponding to orientation g_3. In this second component nuclei form during recrystallization. It was proposed that the heterogeneity is due to mechanical twinning [24]. In order to verify this we have done some polycrystal plasticity texture simulations for rolling of hcp metals, using the self-consistent viscoplastic model [26,27] and assuming the conventional hcp slip and twinning systems and corresponding critical shear stresses (Table 4). Fig. 8 shows pole figures after 50% strain. Individual orientations are divided into two groups: grains with + symbols have not twinned, grains with x symbols have undergone single or multiple twinning. Symbol size is proportional to the average

Table 4
Relative critical resolved shear stresses of slip and twinning systems assumed in polycrystal plasticity simulations for hcp zirconium [21,28]

System	$\{hkl\}$	$\langle uvw\rangle$	c.r.s.s.	Twinning shear
Slip				
Prismatic	$\{10\bar{1}0\}$	$\langle\bar{1}2\bar{1}0\rangle$	0.85	
Basal	$\{0001\}$	$\langle 2\bar{1}\bar{1}0\rangle$	2.5	
Pyramidal $\langle c+a\rangle$	$\{10\bar{1}1\}$	$\langle\bar{1}\bar{1}23\rangle$	2.5	
Twinning				
Tensile	$\{10\bar{1}2\}$	$\langle\bar{1}011\rangle$	1.2	0.167
Compressive	$\{2\bar{1}\bar{1}2\}$	$\langle 2\bar{1}\bar{1}\bar{3}\rangle$	1.7	0.225

Stress exponent $n = 19$ (cf. Fig. 8).

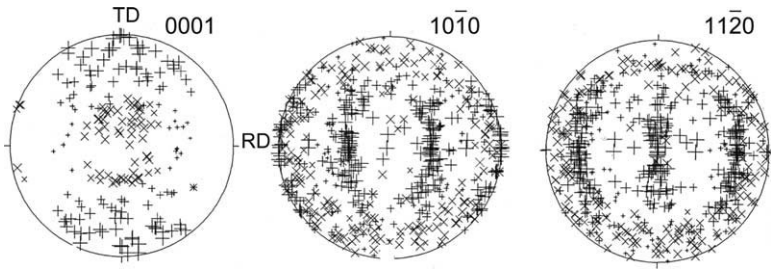

Fig. 8. Self-consistent viscoplastic polycrystal plasticity simulations of texture evolution during rolling for hcp metals. For slip systems and critical resolved shear stresses, see Table 4. Von Mises equivalent strain 50%. Rolling direction (RD) and transverse direction (TD) are indicated. Simulations were done with 2000 orientations but for plotting only 200 were randomly selected. + symbols correspond to untwinned grains, x to twinned grains. Symbol size is proportional to the deformation of individual grains. Pole figures in equal area projection.

Von Mises strain. The main concentration of twinned grains corresponds to the hcp orientations that give the best match for the bcc texture if Burgers relation is applied (component g_3), the untwinned grains correspond to component g_4, where microstructures suggest large grains. It is thus plausible that the highly heterogeneous grains, divided by twin boundaries with high surface energy, act as nucleation sites for precipitation of the bcc phase. These nuclei then grow at the expense of other orientations and ultimately dominate the transformation texture. Growth of these same orientations was identified by in situ SEM investigations [16].

This scenario may explain the grain orientation selection, it does not address the variant selection. For the variant selection it is significant to note that four symmetry variants have (1 1 1) close to the rolling direction and therefore conform to sample symmetry, whereas the other two variants are oblique and this may cause incompatibility between adjacent grains. Morphology may also be important since grains are elongated in the rolling direction and twin boundaries correspondingly aligned. Other factors such as thermal stresses imposed by neighboring grains may also influence the symmetry variant selection during the phase transformation [28,29].

With these new experiments we can not yet contribute much to the question of the memory effect during cooling. It is conceivable that this memory is related to the presence of a small residual fraction of the original hcp phase (5–10%) in the transformed sample as manifested in the diffraction pattern in Fig. 1, bottom. These orientations, dominating the new hcp texture, may be nuclei produced during recrystallization prior to the phase transformation and thus enhancing the recrystallization texture.

Clearly much work remains to be done to understand more fully the mechanisms and processes during the phase transformations in zirconium and titanium. Similar in situ experiments need to be repeated with different texture types and different thermal treatments. We are presently pursuing high temperature texture determinations with neutrons, as well as synchrotron X-rays, extending the method described by Puig-Molina et al. [25]. Synchrotron X-rays have the advantage that heating, cooling, as well as data collection can be done much more rapidly than with neutrons and it should be possible to identify the orientation of the first nuclei that form in the hcp matrix. Neutrons on the other hand provide better grain statistics to assess the bulk texture changes.

5. Conclusions

The texture evolution of hcp and bcc hot-rolled zirconium has been studied in situ during thermal cycling, using time-of-flight neutron diffraction. The overall hcp texture pattern can be described as a mixture of two types: one typical of rolling textures commonly observed in hexagonal metals (preference for $(10\bar{1}0)$ in the rolling direction) and a second one typical of recrystallization (preference for $(11\bar{2}0)$ in the rolling direction). In the initial state the rolling component strongly dominates. As a result of annealing at temperatures between 750 and 950 °C, the component typical of recrystallization increases at the expense of the rolling component, indicating microstructural changes in the course of the experiment before the phase transformation. Computer modeling based on ideal texture components, and using Burgers orientation relation, gives a reasonable match for the bcc texture with the experimental texture pattern if it is assumed that those orientations most typical for the changes during recrystallization transform preferentially into bcc, with a corresponding symmetry variant selection. Comparison with previous microstructure studies on cold worked and annealed titanium sheets [24] and self-consistent viscoplasticity simulations [25] indicates that the orientations that dominate the bcc texture originate from hcp orientations corresponding to those that are most highly susceptible to twinning during rolling, suggesting that the bcc phase may nucleate in highly deformed hcp grains with heterogeneous microstructure and then dominate the texture by preferential growth. The final hcp texture after two heating–cooling cycles resembles the initial rolling texture

modified by the effect of recrystallization. The variant selection in this reverse transformation may be due to growth of untransformed hcp domains.

Acknowledgements

We acknowledge support from NSF, CDAC, IGPP-LANL and LANL-UCDRD. We are thankful to J. Pehl for help during experiments, to T. Holden, L. Lutterotti and C. Tomé for discussions, and to S. Grigull for processing of some data. Comments from two reviewers are much appreciated.

References

[1] Burgers WG. Physica 1934;1:561.
[2] Bollmann W. Crystal defects and crystalline interfaces. Berlin: Springer Verlag; 1970.
[3] Williams AJ, Cahn RW, Barrett CS. Acta Metall 1954;2:117.
[4] Gaunt P, Christian JW. Acta Metall 1959;7:529.
[5] Jourdan C, Gastaldi P, Marzo P, Grange G. J Mater Sci 1991;26:4355.
[6] Wang FM, Ingalls R. Phys Rev 1998;57B:5647.
[7] Pinsook U, Ackland GJ. Phys Rev B 1999;59:13642.
[8] Morris RR, Ho KM. Phys Rev B 2001;63:224116.
[9] Nishiyama Z. Martensitic transformation. New York: Academic Press; 1978.
[10] Ciurchea D, Pop AV, Gheorghiu C, Furtuna I, Todica M, Dinu A, Roth M. J Nucl Mater 1996;231:83.
[11] Gey N, Humbert M, Moustahfid H. Scripta Mater 2000;42:525.
[12] Gey N, Humbert M. Acta Mater 2002;50:277.
[13] Gey N, Gautier E, Humbert M, Cerqueira A, Bechade JL, Archambault P. J Nucl Mater 2002;302:175.
[14] Zhu ZS, Gu JL, Liu RY, Chen NP, Yan MG. Mater Sci Eng A 2000;280:199.
[15] Inakazu N, Inoue H. J Jap Inst Met 1988;52:18.
[16] Seward GGE, Prior DJ, Wheeler J, Celotto S, Halliday DJM, Paden RS, Tye MR. Scanning 2002;24:232.
[17] Wenk HR, Lutterotti L, Vogel S. Nucl Instrum Methods A 2003;515:575.
[18] Matthies S, Vinel GW. Phys Stat Solidi (b) 1982;112:K111.
[19] Lutterotti L, Matthies S, Wenk HR, Schultz AJ, Richardson JW. J Appl Phys 1997;81:594.
[20] Pawlik K. Phys Stat Solidi (b) 1986;134:477.
[21] Wenk HR, Matthies S, Donovan J, Chateigner D. J Appl Cryst 1998;31:262.
[22] Philippe MJ, Serghat M, Van Houtte P, Esling C. Acta Metall Mater 1995;43:1619.
[23] Naka S, Mardon JP, Dervin P, Pernot M, Penelle R, Lacombe P. J Less Common Metals 1977;56:277.
[24] Wagner F, Bozzolo N, Van Landuyt O, Grosdidier T. Acta Mater 2002;50:1245.
[25] Puig-Molina A, Wenk HR, Berberich F, Graafsma H. Z Metallk 2003;11:1199.
[26] Lebensohn RA, Tomé CN. Acta Metall 1993;41:2611.
[27] Tomé CN, Canova GR. In: Kocks UF, Tomé CN, Wenk H-R, editors. Texture and anisotropy Preferred orientations in polycrystals and their effect on materials properties. 2nd ed. Cambridge: Cambridge University Press; 2000. p. 466.
[28] Gloaguen D, Francois M, Guillen R, Royer. J Acta Mater 2002;50:871.
[29] Pang JWL, Holden TM, Turner PA, Masson TE. Acta Mater 1999;47:373.